Three-Dimensional EIT Imaging of Breast Tissues: System Design and Clinical Testing

Vladimir A. Cherepenin, *Member, IEEE*, Alexander Y. Karpov, Alexander V. Korjenevsky*, *Member, IEEE*, Vladimir N. Kornienko, Yury S. Kultiasov, Mikhail B. Ochapkin, Olga V. Trochanova, and J. David Meister, *Member, IEEE*

***Abstract*—Results of development and testing of the new medical imaging system are described. The system uses a planar array consisting of 256 electrodes and enables obtaining images of the three-dimensional conductivity distribution in regions below the skin's surface up to several centimeters deep. The developed measuring system and image reconstruction algorithm can be used for breast tissue imaging and diagnostics, in particular for malignant tumor detection. Examples of tomographic images obtained *in vivo* during clinical tests are presented. The mammary gland, being an organ-target, alters at the background with such physiological events as menstrual cycle, pregnancy, lactation, and postmenopause. The objectives of this paper include estimation of the possibilities of electrical impedance mammography for investigation of mammary glands' state among women with different hormonal status. We found that electrical impedance mammograms from different groups had clear visual distinctions and statistically significant differences in mammary glands' conductivity. Our data on conductivity distribution in the mammary gland during different physiological periods will allow us to use it as normal values in the future, to continue this research on mammary glands with different pathology.**

***Index Terms*—Breast tissue diagnostics, electrical impedance tomography, three-dimensional imaging.**

I. Introduction

THE application of nonionizing fields and radiation for breast diagnostics aimed at early tumor detection is a task of current interest for biomedical electronics research. Electrical properties of many tumors and in particular the malignant tumors of the mammary gland significantly differ from the properties of surrounding sound tissues. This fact can be used for the detection and localization of such tumors [1], [2]. The use of electrical impedance tomography (EIT) is a promising application for such detection. Its main advantages include: 1) absolute safety of examination; 2) high potential for significant correlation of biological tissues electrical impedance with their physiological state; 3) compact and inexpensive equipment; and 4) simple examination procedure. Disadvantages of the method are low resolution which falls significantly with increased distance beneath the patient's body surface, as well as the fact that in many instances only so-called dynamic imaging can be fulfilled (i.e., the reconstruction of images of a conductivity change between two consequent measurements). The application of EIT in mammography requires special designs of the measuring system and image reconstruction algorithm. Although there are research projects using common two-dimensional (2-D) EIT with electrodes arranged in a ring [3], we consider the imaging of a three-dimensional (3-D) distribution of conductivity essential to breast diagnostics. This requires applying a 2-D array of electrodes for data acquisition and corresponding reconstruction software, such as suggested in [4], to provide a 3-D image reconstruction.

We have developed a measuring system and image reconstruction algorithm that enables imaging the spatial distribution of conductivity of the medium contiguous to the surface by using a set of electrodes in the form of a planar array on the surface. The visual result is several cross sections of the medium, which are parallel to the electrode array and located at different depths. The paper describes a new measuring system where we have realized some ideas, which appeared after the first model of electrical impedance mammograph as described in [5] had been clinically tested. The preliminary tests of the device demonstrated reproducibility and potential clinical value of images being obtained.

Mammary tissue is an important part of the reproductive system of the female organizm; its tissues are targets for the active effect of sexual steroid hormones, hormones of hypophysis, and other endocrine glands. During such physiological events as menstrual cycle, pregnancy, lactation, and menopause, mammary glands are affected by sexual hormones according to the type of secretion. Nowadays, ultrasound is sometimes used for definition of hormone-dependent changes in breast tissue.

Earlier we have demonstrated that EIT gives the opportunity to obtain an image and digital expression of the mamma's state with cancer [5].

In this research, we tried to estimate possibilities of using EIT in the examination of mammary glands with different hormone's status.

Manuscript received August 30, 2001; revised March 26, 2002. This work was supported by Technology Commercialization International, Inc. *Asterisk indicates correspnding author.*

V. A. Cherepenin is with the Institute of Radio-Engineering and Electronics of Russian Academy of Sciences, Moscow 101999, Russia.

A. Y. Karpov is with the Clinical Hospital No 9, Yaroslavl 150033, Russia.

*A. V. Korjenevsky is with the Institute of Radio-Engineering and Electronics of Russian Academy of Sciences, Mokhovaya 11-7, Moscow 101999, Russia (e-mail: korjenevsky@cplire.ru).

V. N. Kornienko and Y. S. Kultiasov are with the Institute of Radio-Engineering and Electronics of Russian Academy of Sciences, Moscow 101999, Russia.

M. B. Ochapkin and O. V. Trochanova are with the Yaroslavl State Medical Academy, Yaroslavl 150000, Russia.

J. D. Meister is with Technology Commercialization International, Inc., Albuquerque, NM 87110 USA.

Publisher Item Identifier 10.1109/TMI.2002.800602.

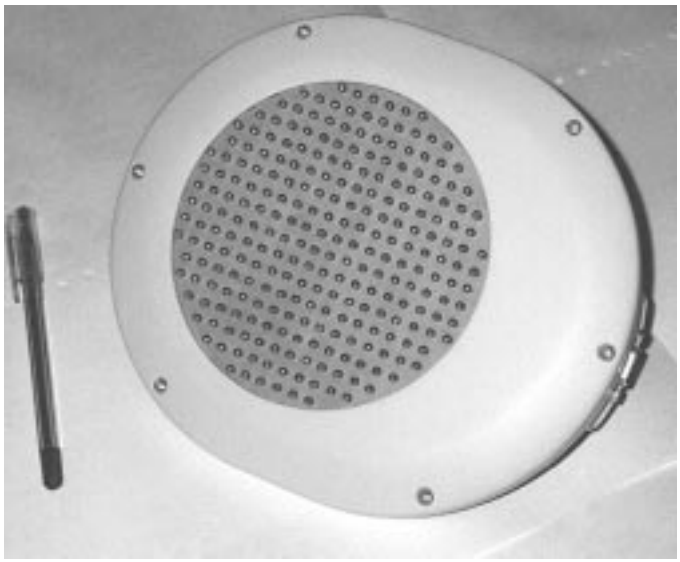

Fig. 1. View of the electrodes array.

II. Materials and Methods

A. Measuring System

The measurements are carried out using a 256-electrode array. The electrodes are arranged in a round matrix with a diameter of 12 cm (Fig. 1). During an examination, the plane of electrodes is pressed against the breast, flattening it toward the chest. This increases the number of electrodes in contact with the breast and decreases the thickness of the tissue layer to be measured. The conversion, from a square array applied in a previous design to a round array, allowed a substantial increase in the electrodes' utilization factor. There are no corner areas in the new system. In such the areas, the electrodes had practically no contact with a patient's skin. Also, the diameter of the array and the number of electrodes being the same, their density increased (the distance between adjacent electrodes became less), this fact has promise for increasing the system's resolution. Two remote electrodes are attached to patient's wrist by means of a clip. The first remote electrode acts as a common current source electrode; the other remote electrode is a potential difference detector reference electrode. Standard extremity electrocardiogram electrodes are used.

The current source consists of a microprocessor controlled digital-to-analog (D/A) converter and a voltage–current converter. A voltage threshold detector connected to the current source output permits the detection of bad contacts with a patient's skin (high contact impedance) and, therefore, improves the image reconstruction process. The criterion of a bad contact is when the output voltage exceeds threshold, which is below the limits of the linearity of the current source. In the case of active load, it corresponds to the resistance exceeding approximately 10 kΩ. During the measurement process, the output 256-channel analog multiplexer switches a single lead from the current source to activate a single electrode in the electrode array. The current source circuit is closed through a patient's body and the grounded remote electrode positioned on a patient's wrist. The current frequency can be changed by means of the embedded software; the maximum operating frequency of the apparatus is 110 kHz. Due to the primary capacitive nature of the skin impedance, it is easier to provide sufficient contact of the electrodes with the body without putting high conductive media on the skin at higher frequencies. On the other hand, the parasitic capacitances limit the accuracy of measurements at high frequency. After the system tests, the operating frequency of 50 kHz has been chosen as optimal because of convenience of measurements (it is possible to make measurements with only slightly moistened skin) and the low level of spurious couplings. The amplitude of rectangular waveform current used in the described measuring system is 0.5 mA.

The potential difference detector consists of an integral instrumentation amplifier with the controlled gain factor, a passive lowpass filter, analog-to-digital (A/D) converter and the embedded software for digital signal processing. During the measuring process, one of the differential inputs of the instrumentation amplifier is switched to a single electrode in the electrode array by means of 256-channel multiplexer. The other amplifier's input is connected to the remote reference electrode positioned on a patient's wrist. The D/A converter output of the contact potential compensation system is connected to the instrumentation amplifier bias input. Before starting measurements on the next electrode, the system measures the contact potential and calculates the code, which is necessary to deliver to this D/A converter for compensation. If the system is not able to compensate the contact potential difference after several attempts, the electrode is marked as faulty in the corresponding table. A 14-bit A/D converter (actual conversion accuracy is 13 bit) is applied in the system. Digital signal detection, device control, and communication with a host computer are carried out by means of the embedded single-chip microcontroller (Atmel's AT90S8515).

The sequence of measuring system operation is the following. The potential difference detector is switched by the multiplexer to the first array electrode, the procedure of contact potential difference compensation is carried out, after that the current source successively switches to each of the remaining electrodes of the array and measurements are fulfilled. The instrumentation amplifier's gain factor is adjusted depending on the distance between the injecting and the measuring electrodes for maximum utilization of A/D converter's dynamic range. After that the cycle is repeated to measure another electrode. A switch-over of the measuring electrode in the external (slow) cycle decreases influence of transients, related with contact potential jumps on the detector's input. A whole data set used for 3-D conductivity reconstruction consists of 65 280 results of measurements. Data processing and measurement process initiating are carried out by means of a personal computer connected to the device by RS-232 communication channel with a 115 200 bit/s rate. Data transmission and measurement processing are being implemented simultaneously, thus, a full measurement cycle takes less than 20 s.

B. Image Reconstruction

The method of backprojection along hemispherical equipotential surfaces of the electric field is applied for 3-D conductivity reconstruction in a medium near the electrodes array. The 3-D imaging allows improved localization of findings without carrying out multiple investigations. In particular,

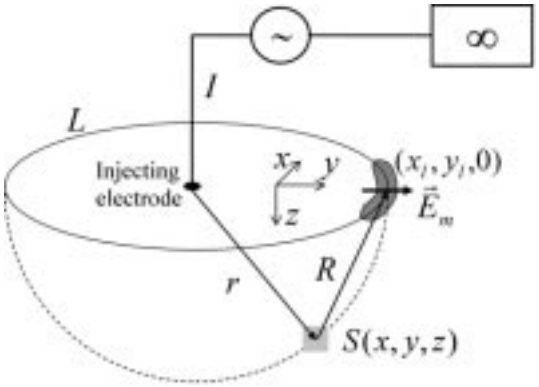

Fig. 2. Reconstruction of 3-D distribution of conductivity.

it gives information regarding the depth of the detected abnormalities and decreases the masking of deeper objects. The key elements of the algorithm have been described in [5]. In addition, it should be mentioned that the array form has been changed from square to round allowing a slight correction of the projecting procedure. Besides, the weight coefficients applied in projecting have been optimized to equalize the tomographic system's sensitivity in depth. While the reconstruction algorithm provides static imaging, it does not provide the absolute values of conductivity, and reconstructed conductivity is presented in arbitrary units. The conductivity value S in the point (x, y, z) is calculated according to

$$S(x,y,z) = 1 + W_1(z) \sum_i \frac{1}{\int\limits_{L(x,y,i)} W_2(l)dl} \times \int\limits_{L(x,y,i)} \frac{W_2(l)(E_r(l) - E_m(l))}{E_r(l)} dl$$

$$W_2 = \frac{1}{R^4} = \frac{1}{((x - x_l)^2 + (y - y_l)^2 + z^2)^2}$$

where W_1 is monotone increasing weight function, which equalizes sensitivity in depth z, i is the number of the injecting electrode, and $L(x, y, i)$ is the line of intersection of the equipotential surface with the plane $z = 0$, on which the electrodes are arranged. The components of the measured electric field vector $\vec{E}_m$ are calculated at the nodes of the grid between the electrodes as the potential differences between adjacent electrodes in the x and y directions. Then these components are linearly interpolated to the current point of integration on the line L. The reference intensity of the electric field E_r corresponds to a homogeneous medium and is calculated numerically. See Fig. 2 for detailed definitions of geometrical values used in the equation.

The reconstruction results in electrical impedance images of seven cross-sectional slices of the investigated medium parallel to the electrodes' plane each with an 8-mm depth step starting at 4 mm from the surface (see Fig. 3). The size of each image (from left to right and from bottom to top) represents the diameter of the electrodes array (12 cm). There are several tools for additional processing of obtained images. To increase contrast or to make some parts of an image more distinct, it is possible to change or adjust the gray scale applied for conductivity

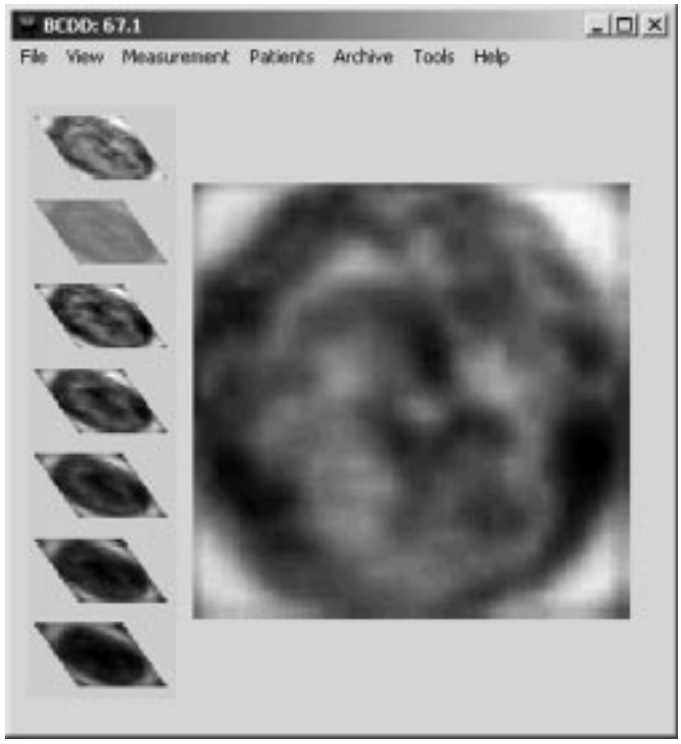

Fig. 3. EIT cross sections.

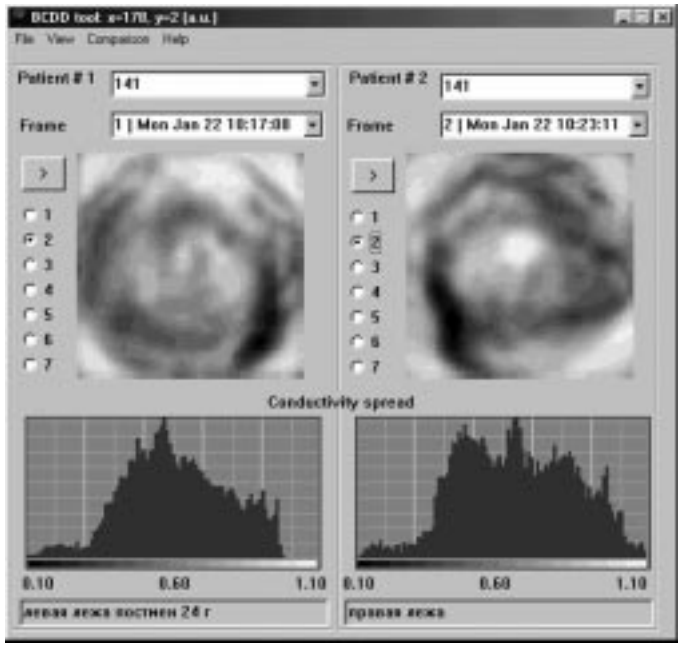

Fig. 4. Comparison of images and histograms of normal breast (left) and breast with tumor (right) of the same patient (aged 70, 24 years in menopause).

imaging. It is also possible to compare two images, e.g., images of left and right breasts both visually and using frequency diagrams of image brightness distribution (histograms); see illustration in Fig. 4. To the latter case, the Kolmogorov–Smirnov nonparametric statistical criterion can be applie to determine the difference between histogram under estimation and, e.g., a histogram of standard image considered to be a norm. There is also a possibility of creating images that look similar to the images

produced by the T-Scan [2] system, i.e., without depth differentiation. We call this the "integral view."

C. Clinical Measurement

Fifty-seven women-volunteers from 18 to 61 years old were investigated. They were divided on five clinical groups: the first group consisting of 12 women from 18 to 45 years old at the first menstrual cycle phase (from 1 to 10 days); the second group consisting of 12 women from 18 to 45 years old at the second menstrual cycle phase (from 16 to 28 day); the third group consisting of 14 women from 18 to 39 years at pregnancy (37–40 weeks); the foutth group consisting of 14 women from 18 to 39 years at lactation period (3–5 days after labor); and the fifth group consisting of five women from 47 to 61 years at postmenopause (more than one year).

Criteria for choosing woman-volunteers for investigation were the following: absence of patient's complaints on mammary glands, absence of mammary gland diseases, normal 28-day menstrual cycle, absence of alarming somatic and gynecological history, absence of pathological alterations at ultrasound investigation of mammary glands, and no hormonal contraception.

The breast scans were made in supine and standing positions. Duration of one patient investigation (electrodes application, mammogram registration, image processing) was about 10–15 min.

The analysis of obtained electrical impedance mammograms (EIM) included: visual image estimation, evaluation of general parameters of conductivity and its variability (mean value, standard deviation, and maximum and minimum values); varying statistical methods (Students criteria); comparison of conductivity values obtained during investigation at different frequencies.

III. Results

A. Laboratory Tests

To estimate and optimize the instrument's parameters, the tomographic system has been tested by means of a dielectric tank filled with water with test objects immersed. Examples of such imaging are demonstrated on the Figs. 5 and 6. On Fig. 5 the images of cross sections of the glass (tube with bottom) immersed in the tank are shown. Fig. 6 demonstrates the view of a small ball made from aluminum foil, which is placed in the tank at some distance from the device.

Due to the primary capacitive nature of the skin impedance, it is easier to provide sufficient contact of the electrodes with the body without putting high conductive media on the skin at higher frequencies. On the other hand, the parasitic capacitances limit the accuracy of measurements at high frequency. The tank tests have demonstrated that the visualization quality (resolution and sensitivity) remains stable at frequencies up to 60 kHz. For higher frequencies, the influence of artifacts became apparent.

Increasing averaging time during measurements has no influence on the visualization results. This fact indicates that image degradation at higher frequencies is due to systematic errors, probably related with spurious couplings arising from the crosstalk and stray capacitances in the multiplexers and other input circuits of the measuring system. The working frequency of 50 kHz was considered optimal and was used in further clinical investigations.

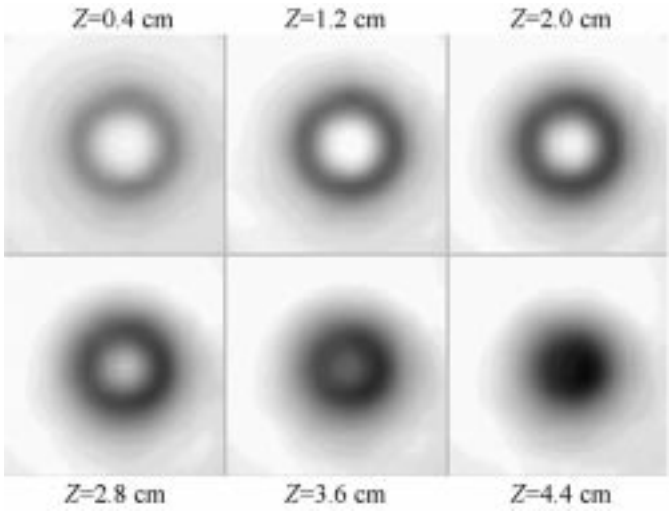

Fig. 5. Tank imaging: the glass (tube with bottom) is immersed to the water vertically, diameter of the glass is 5 cm, height is 9 cm, distance from the electrodes is 1 cm; Z is depth from the electrodes.

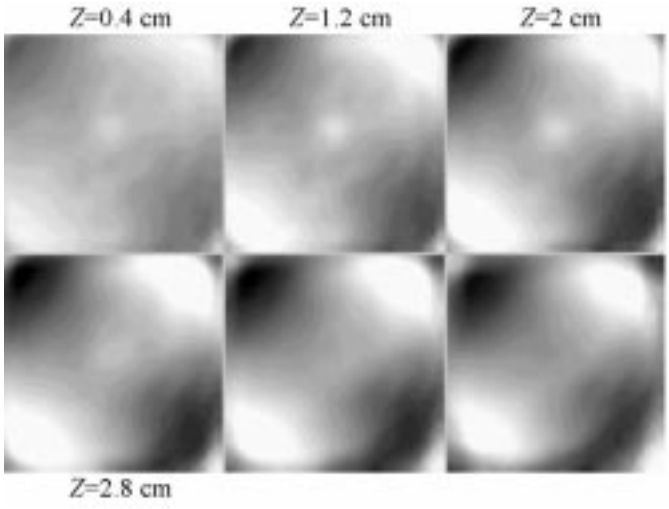

Fig. 6. Tank imaging: the ball from aluminum foil (white spot near the center), diameter of the ball is 0.8 cm, distance from the electrodes is 2 cm; Z is depth from the electrodes.

B. Clinical Results

During the first clinical tests, it was established that the system could visualize breast anatomic structures, which are peculiar for every patient, including areas of pathologic changes that appear in images mostly as white spots (increased conductivity). The imaging results have good reproducibility not only for several measurements taken during one examination but also for measurements taken after significant periods of time.

1) EIT Images of Mammary Glands: Electrical impedance images present the mammary gland conductivity in grey scale; change from dark to light corresponds to change from low electric conductivity to high. For correct image estimation, we compared mammograms from the same cross section (scanning plane).

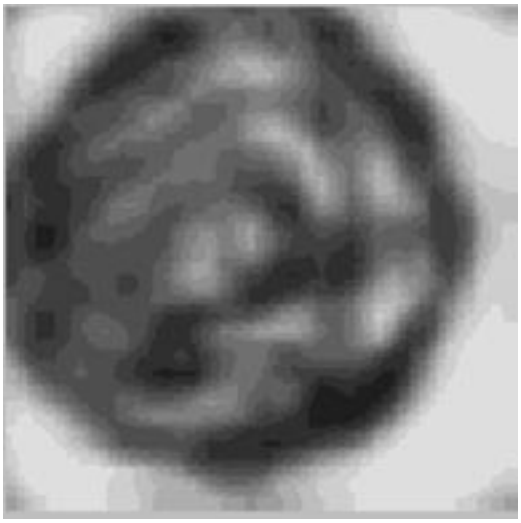

Fig. 7. EIT image of normal breast in the first phase of menstrual cycle (age 22, eighth day in cycle).

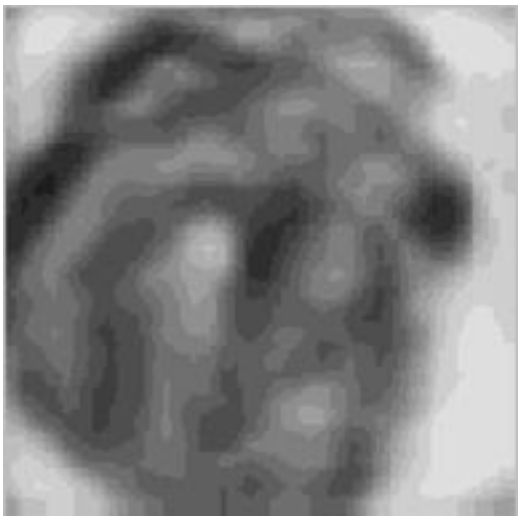

Fig. 8. EIT image of normal breast in the second phase of menstrual cycle (age 34, 22nd day in cycle).

In the first phase of the menstrual cycle (1–10 days), cell proliferation occurs in the duct-lobe structure under the influence of estrogen. EIM image of mammary gland in the first phase is characterized by smooth allocation of grey tones and absence of symptomatic node (Fig. 7). "Mosaic" structure of images is explained by its complex anatomical composition.

In the second phase (16–28 days), because of estrogen receptors down-regulation in mammary gland epithelium under the influence of a rising quantity of progesterone, the gradual decreasing of cell proliferation begins. Then evolution and differentiation of alveoli and secretory transformation of gland tissue follows. At the end of the first phase, the apoptosis takes place. EIM images of the mammary gland in the second phase (Fig. 8) are also characterized by smooth allocation of grey tones and absence of symptomatic node; moreover there are more light tones as compared with the first phase (Fig. 7). The presence of light tones can be explained by the increased quantity of secrete or liquid in breast tissues because of changes in gland epithelium causing the tissue conductivity to increase.

At pregnancy (37–40 weeks), the combined influence of progesterone, prolactin and estrogens of placenta are accompanying the morpho-functional preparation for lactation. At the end of pregnancy, mamma consists of glandary tissue because of developing lobules, decreased connective tissue and increased volume of ducts. EIM images of the mammary gland at the end of pregnancy are characterized by smooth allocation of grey tones and presence of light tones (Fig. 9).

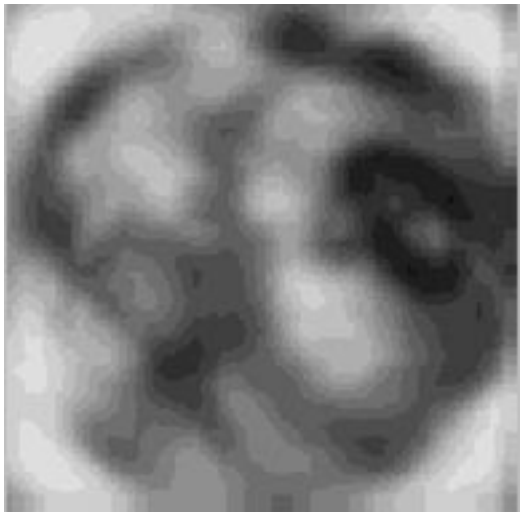

Fig. 9. EIT image of breast at pregnancy (age 34, 39th week in pregnancy).

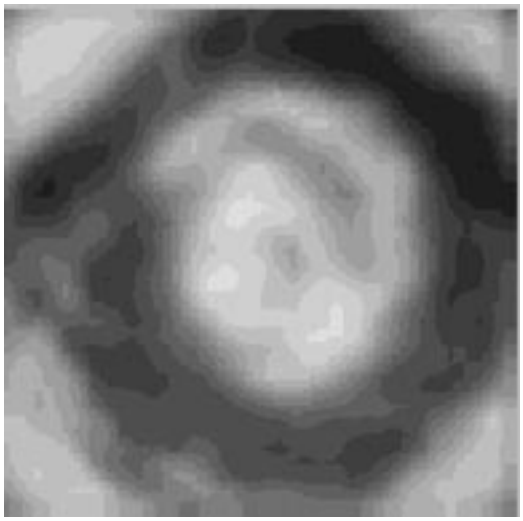

Fig. 10. EIT image of breast at lactation period (age 34, third day after labor).

At the end of pregnancy and during the first days after labor—due to the abrupt decrease of the placenta's estrogen level, there is the prolactin peak ejection, which switches on the lactation mechanism. At lactation, EIM image are characterized by a distribution of dark tones on the periphery and contrasting light tones in the center (Fig. 10). This reflects milk accumulation in the main ducts and increased tissue conductivity.

During postmenopause, when the level of estrogens and gestagens decrease, the replacement of glands by fat, connective tissue, and hyaline tissue starts. EIT image of the mammary gland during menopause looks lighter with contrast changes to dark tones. No symptomatic nodes are present (Fig. 11).

2) Conductivity of Mammary Glands at Different Conditions: For estimation of mammary gland tissue conductivity, we used average values from the second scanning plane (1.2-cm depth). Conductivity is presented in conventional units.

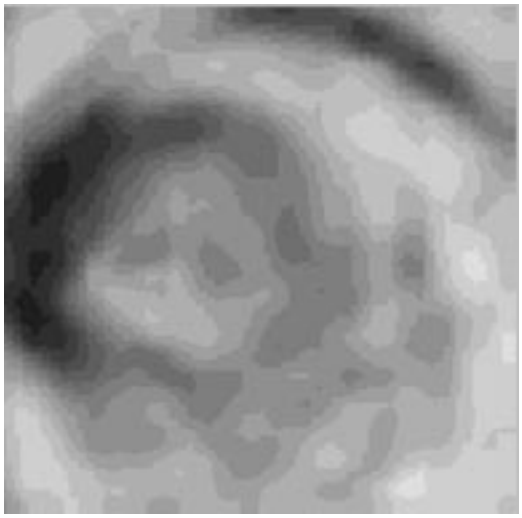

Fig. 11. EIT image of breast at menopause (age 52, three years in menopause).

Conductivity of mamma in the supine position is higher in all groups but we did not find statistically significant differences ($p > 0.05$). In further computations, we used conductivity values measured from supine position.

Tissue conductivity of left and right mammary glands in all groups does not differ ($p > 0.05$).

We did not find statistically significant differences in groups 1, 2, 3, and 4 ($p > 0.05$). There is a difference in conductivity in group 5 relative to groups 1, 2, 3, and 4 ($p < 0.001$).

In this research, we compared results of measurements carried out using a first-generation system operating at 10 kHz with the new system working at 50 kHz, comparing them as current of low and high frequency. Because of different reconstruction algorithms it would be incorrect to compare absolute results of conductivity obtained with different systems. It would be more objective to compare the percent of increase/decrease of mean conductivity of mammary glands of women from different groups at one frequency, to percent increase/decrease of mean conductivity at another frequency. There is an interesting comparison of the percent of increase of mean conductivity of mammas from women from group 1 and 2 to group 5 while using different frequency. While using the 10 kHz current there is an increase in mean conductivity by 11%, but at 50 kHz, the increase in conductivity is 52%– 64% (Fig. 12). It can be explained by the dispersion properties of connective tissue and hyaline stroma developing in mammary glands at postmenopause.

IV. Discussion

The change in form of the electrode array as well as the transition to digital signal processing improved the measuring system characteristics. Also, the device design has been simplified by reducing the number of precision analog components.

The results of clinical tests allow stating that the device, operating at a frequency near 50 kHz, is capable of visualizing the electrical impedance structure of breast tissues and obtaining results that are of clinical value. Stepping up the device operation frequency to 60 kHz or more results in impairment of image

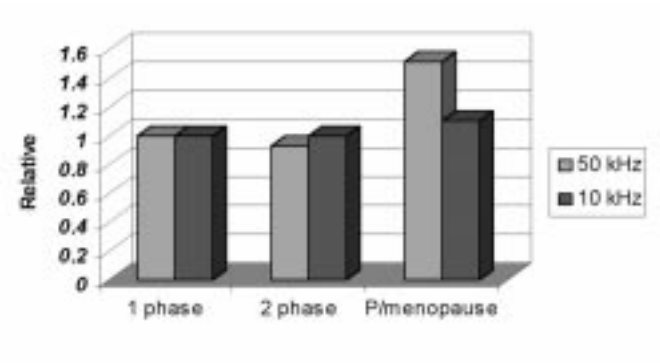

Fig. 12. Changes of mammary conductivity at different frequencies (50 kHz and 10 kHz). The data is normalized to one for the first group at both frequencies.

quality. This is first of all associated with the spurious capacitances in the measuring system's input circuits.

Two-frequency measurements, for example, at 10 and 50 kHz enable frequency variance estimation of abnormalities found in electrical impedance images that may simplify their identification. Such two-frequency measurements can be realized by means of the measuring system described in the paper.

EIT images of mammary glands seem to be the same at the first and second phases of the menstrual cycle and also at the period of pregnancy. During lactation, light colors at the center of the image reflect increased conductivity due to the milk content in the galactophorous ducts. EIT images at menopause are visually distinguished from the images during fertility.

Conductivity analysis shows that mean conductivity of mamma for a healthy woman in the supine position is higher than in a standing position. It may be related to hemodynamic changes when changing position of the patient. The conductivity of mammary glands in a healthy woman is the same at first and second phase of a 28-day menstrual cycle. The conductivity increase in postmenopausal breasts observed in the experiments can be explained by involution processes. These processes include not only replacing the mammary gland with fat, but also increasing the connective and hyaline tissue.

Our data on conductivity of mamma's tissue in women during different physiological periods allows us to use the information as normal values in the future and continue this research on mammary glands with different pathology.

References

[1] A. J. Surowiec, S. S. Stuchly, J. R. Barr, and A. Swarup, "Dielectric properties of breast carcinoma and the surrounding tissues," *IEEE Trans. Biomed. Eng.*, vol. BME-35, pp. 257–262, 1988.

[2] M. Assenheimer, O. Laver-Moskovitz, D. Malonek, D. Manor, U. Nahaliel, R. Nitzan, and A. Saad, "The T-SCAN TM technology: electrical impedance as a diagnostic tool for breast cancer detection," *Physiol. Meas.*, vol. 22, pp. 1–8, 2001.

[3] A. Hartov, T. E. Kerner, M. T. Markova, K. S. Osterman, and K. D. Paulsen, "Dartmouth's next generation EIS system: preliminary hardware considerations," *Physiol. Meas.*, vol. 22, pp. 25–30, 2001.

[4] J. L. Mueller, D. Isaacson, and J. C. Newell, "A reconstruction algorithm for electrical impedance tomography data collected on rectangular electrode arrays," *IEEE Trans. Biomed. Eng.*, vol. 46, pp. 1379–1386, Nov. 1999.

[5] V. Cherepenin, A. Karpov, A. Korjenevsky, V. Kornienko, A. Mazaletskaya, D. Mazourov, and D. Meister, "A 3D electrical impedance tomography (EIT) system for breast cancer detection," *Physiol. Meas.*, vol. 22, pp. 9–18, 2001.